

pubs.acs.org/JPCB Article

# Biophysical Rationale for the Selective Inhibition of PTP1B over TCPTP by Nonpolar Terpenoids

Anika J. Friedman, Hannah M. Padgette, Levi Kramer, Evan T. Liechty, Gregory W. Donovan, Jerome M. Fox,\* and Michael R. Shirts\*

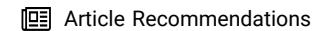


Cite This: J. Phys. Chem. B 2023, 127, 8305-8316



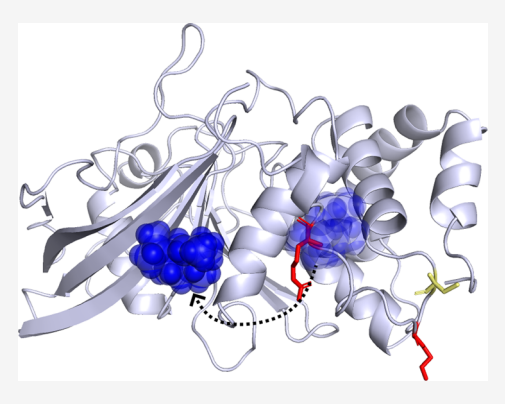
**ACCESS** I

III Metrics & More



s Supporting Information

**ABSTRACT:** Protein tyrosine phosphatases (PTPs) are emerging drug targets for many diseases, including cancer, autoimmunity, and neurological disorders. A high degree of structural similarity between their catalytic domains, however, has hindered the development of selective pharmacological agents. Our previous research uncovered two unfunctionalized terpenoid inhibitors that selectively inhibit PTP1B over T-cell PTP (TCPTP), two PTPs with high sequence conservation. Here, we use molecular modeling, with supporting experimental validation, to study the molecular basis of this unusual selectivity. Molecular dynamics (MD) simulations suggest that PTP1B and TCPTP share a h-bond network that connects the active site to a distal allosteric pocket; this network stabilizes the closed conformation of the catalytically essential WPD loop, which it links to the L–11 loop and neighboring  $\alpha 3$  and  $\alpha 7$  helices on the other side of the catalytic domain. Terpenoid binding to either of two proximal C-terminal sites—an  $\alpha$  site and a  $\beta$ 



site—can disrupt the allosteric network; however, binding to the  $\alpha$  site forms a stable complex only in PTP1B. In TCPTP, two charged residues disfavor binding at the  $\alpha$  site in favor of binding at the  $\beta$  site, which is conserved between the two proteins. Our findings thus indicate that minor amino acid differences at the poorly conserved  $\alpha$  site enable selective binding, a property that might be enhanced with chemical elaboration, and illustrate more broadly how minor differences in the conservation of neighboring—yet functionally similar—allosteric sites can affect the selectivity of inhibitory scaffolds (e.g., fragments).

# INTRODUCTION

An important challenge in the development of therapeutic inhibitors is the joint optimization of affinity and selectivity. In a standard workflow, a medicinal chemist might increase the binding affinity of a compound for a drug target by increasing its nonpolar surface area, but large nonpolar compounds often bind nonspecifically, a potential source of toxic side effects.<sup>1,2</sup> Our previous work suggests that some nonpolar terpenoids can exhibit selective interactions with protein tyrosine phosphatases (PTPs).3,4 Of course, nonpolar terpenoids are not generally useful as drugs; they have poor metabolic stability and low solubility, which limits bioavailability. Nonetheless, they are promising scaffolds for drug development. Paclitaxel and artemisinin are notable examples of highly effective terpenoid-based therapeutics.<sup>6,7</sup> This study uses selective terpenoid inhibitors of PTPs to study the molecular basis of selective binding between nonpolar compounds and proteins, a class of interactions that remains challenging to exploit in rational drug design.

The human genome contains ~107 PTPs, of which ~38 are tyrosine-specific—or "classical"—PTPs that share a highly conserved catalytic domain.<sup>8</sup> Pronounced structural conservation at the active site of these PTPs has made the development of selective inhibitors difficult and driven researchers to focus

on less conserved allosteric sites. <sup>9,10</sup> PTP1B provides a prominent example. This enzyme is a long-standing target for treating type 2 diabetes, obesity, and cancer <sup>11–18</sup> and has emerged more recently as a promising immuno-oncology target. <sup>19</sup> Its structural similarity to T-cell PTP (TCPTP), which shares an 80% sequence identity, has focused medicinal chemistry efforts on a C-terminal allosteric site, a promising source of selective interactions with small molecules. Intriguingly, even this site has relatively high structural conservation, which enhances the difficulty of developing selective compounds (Figure S1). A detailed understanding of different mechanisms of selective allosteric inhibition could yield new approaches to improve molecular selectivity.

The promise of PTP1B as a drug target has driven extensive inhibitor development. Most inhibitory compounds bind to the active site, but several bind to the allosteric site. The most well-studied allosteric inhibitor is the benzofuran 3-(3,5-dibromo-4-

Received: June 5, 2023
Revised: September 6, 2023
Published: September 20, 2023





hydroxy-benzoyl)-2-ethyl-benzofuran-6-sulfonic-acid-(4-(thiazol-2-ylsulfamyl)-phenyl)-amide, referred to here as BBR, which was discovered in an early high-throughput screen and has comparable selectivity to other potent PTP1B inhibitors. Upon binding to PTP1B, BBR engages in both  $\pi$ -stacking interactions with a nonconserved PHE280 residue and h-bonds with neighboring residues in the C-terminal allosteric pocket. In prior work, we used X-ray crystallography, MD simulations, and mutational analysis to show that BBR and amorphadiene (AD), a completely nonpolar terpenoid, disrupt the allosteric network of PTP1B in a similar manner. AD and  $\alpha$ -bisabolene (AB), a chemically similar compound, are surprisingly selective for PTP1B, which they inhibit 5–8× more potently than TCPTP, a selectivity similar to BBR 4,20 (Figure 1). In general, AD and AB are intriguing inhibitors

**Figure 1.** Chemical structures of two small terpenoid inhibitors: (A) amorphadiene (AD) and (B)  $\alpha$ -bisabolene (AB).

because they cannot form h-bonds or other specific interactions and must therefore exhibit a mechanism of selectivity distinct from that of BBR. Understanding the mechanism by which nonfunctionalized inhibitors achieve both moderate potency and isoform selectivity could inform the optimization of allosteric inhibitors for both PTP1B and TCPTP.

In prior work, we used molecular modeling to study how AD inhibits PTP1B. Our simulations showed that AD can sample two neighboring regions of the C-terminal allosteric site, both of which require a disordered  $\alpha$ 7 helix to form a stable complex. In forming this complex, AD disrupts a h-bonding network that stabilizes the closure of the catalytically essential WPD loop. This previous modeling work helped explain the mechanisms of AD binding and inhibition, but it did not shed light on the molecular basis of its selectivity for PTP1B over TCPTP, which has sequence differences in both the  $\alpha$ 6 and  $\alpha$ 7 helices, but not in the  $\alpha$ 3 helix, the residues involved in the putative h-bond network, or the active site.

Here, we used molecular modeling to study the mechanistic basis of selective inhibition by AD and AB, and we used in vitro kinetic assays to test several predictions. Our work seeks to determine how minor differences in the sequences of PTP1B and TCPTP might cause differences in either binding affinity or allosteric modulation. Our use of two terpenoid inhibitors helps us test, and expand on, our previously proposed mechanism of inhibition The direct comparison of binding to two PTPs helps us answer three pressing questions:

 Does an analogous h-bonding network stabilize the closed conformation of the WPD loop in both PTP1B and TCPTP?

- If present, is the allosterically influential h-bond network of TCPTP susceptible to modulation through disruption of the  $\alpha 3-\alpha 7$  interface, as it is in PTP1B?
- Do nonfunctionalized terpenoids such as AD and AB exhibit conserved binding modes and inhibitory mechanisms for both PTP1B and TCPTP?

# MATERIALS AND METHODS

Molecular Dynamics (MD) Simulations. We prepared PTP1B and TCPTP for MD simulations by starting with four X-ray crystal structures: apo PTP1B (PDB code: 1SUG), apo TCPTP with a closed WPD loop and an ordered  $\alpha$ 7 helix (PDB code 7F5N), apo TCPTP with an open WPD loop and a disordered-unresolved  $\alpha$ 7 helix (PDB code 1L8K), and PTP1B in complex with AD (PDB code: 6W30). We used these structures as initial conformations after postprocessing. 4,23-25 For each structure, we removed crystallized waters, glycerol, and Mg<sup>2+</sup>, adjusted the protonation state to a pH of 7 using the H++ web server, added Na<sup>+</sup> ions to neutralize the net charge, and hydrated the protein with a TIP3P water box, maintaining a minimum distance of 10 Å between the protein or ligand and the periodic boundary. Given routine incorrect predictions by H++, the catalytic CYS215 residues were manually verified to be in the expected deprotonated state for physiological pH conditions.

We carried out MD simulations with GROMACS 2020.4<sup>26</sup> on the Bridges-2 cluster at the Pittsburgh Supercomputing Center. In all simulations, we modeled PTP1B with the AMBER ff 99sb-ildn force field and parameterized AD and AB with the Open Force Field v.1.3.0 "Parsley". 27 All analysis scripts and input parameters can be found in the repository at https://github.com/shirtsgroup/TCPTP. Ligand parameterization scripts can be found in the repository folder "Ligand Parameters". We carried out an energy minimization to 100 kJ/ mol/nm force tolerance and equilibrated the protein in the NVT ensemble at 300 K for 100 ps, followed by equilibration to the NPT ensemble at 300 K and 1 atm for 100 ps. All simulations used the velocity rescaling thermostat28 and Berendsen weak-coupling barostat. Further configuration details for the simulations appear in the repository folder "data/mdp". We ran all MD simulations for 300 ns (unrestrained NPT) and visualized using PyMOL 2.4.2

X-ray crystal structures of PTP1B and TCPTP with the WPD loop in an open conformation have a disordered  $\alpha$ 7 helix that prevents the crystallographic resolution of this helix. We generated conformations of PTP1B with a disordered  $\alpha$ 7 helix by using the procedure and rationale explained in our previous study of PTP1B.3 In this study, we used the same method to generate the disordered conformations of TCPTP with a disordered helix; however, the  $\alpha$ 7 helix on TCPTP was more resistant to destabilization. Following the procedure of the previous study, we applied the same position restraints to residues 1-280 of TCPTP during the local heating procedure and increased temperature linearly from 400 to 500 K over 300 ns. Following these steps, an additional 100 ns of simulation at 500 K was necessary to disorder the  $\alpha$ 7 helix to below 50%  $\alpha$ helicity, where  $\alpha$  helicity is defined as the percent of residues in the  $\alpha$ 7 helix (residues 284–294 for TCPTP), which are in the  $\alpha$  helical conformation as defined by the defined secondary structure prediction (DSSP) algorithm. The increased temperature forces the targeted unrestrained residues to lose their secondary structure as the protein slowly denatures; this

disordering resembles the protein's natural transition but occurs over a faster time scale. We selected three disordered conformations from the final 50 ns of this trajectory. When we initiated PTP1B bound to BBR with an ordered  $\alpha$ 7 helix, the  $\alpha$ 7 helix disordered within 50 ns; however, for analogous simulations with TCPTP, the  $\alpha$ 7 helix plateaued at  $\sim$ 50%  $\alpha$  helicity over 300 ns. We selected two partially disordered conformations from the final 50 ns of the 300 ns trajectory. As a disordered helix has no single "correct" conformation, we used multiplied conformations in our study to better represent an ensemble of disordered structures.

There is no available crystal structure for TCPTP in complex with either AD or AB binding poses; for both, the initial configurations were determined using molecular docking and through PTP1B-AD structure alignment. AutoDock Vina 1.2.0 $^{30}$  was used to perform molecular docking to apo TCPTP structures with a disordered  $\alpha 7$  helix and open WPD loop. For AD docking, the TCPTP structure used was the centroid from clustering on backbone atoms of the apo trajectory of all five generated disordered  $\alpha 7$  helix configurations.

Docking was performed for each of the five structures with a 27 nm<sup>3</sup> search space centered on the crystal binding site of AD to PTP1B, as we were originally operating under the assumption that the ligands would bind to approximately the same location on TCPTP. For docking, a search exhaustiveness of 32 was utilized, and the 15 highest affinity binding modes were generated. Of these 15 modes, all of those determined to be distinct and unlikely to be sampled in the same trajectory were chosen as initial configurations. Distinct conformations were determined based on their proximity to one another as those whose ligand center of mass was within 5 Å are likely to be sampled within the same trajectory given the center-of-mass (COM) root-mean-square deviation (RMSD) of AD is approximately 7 Å. This procedure produced 4-5 binding locations, depending on the TCPTP structure used. For AB, only the two disordered  $\alpha$ 7 helix conformations, which lead to stable AD binding in at least one initial configuration, were used for docking; otherwise, the procedure was identical.

None of the initial binding poses generated by docking were in the crystal binding location for PTP1B, and thus an additional configuration was added, with each ligand placed in the AD crystal binding location as determined by aligning the protein backbone. Minor modifications were made (movements of <1 Å) to account for steric clashes between the ligand and protein, which produced infinite energies during minimization. All initial configurations were initially run for 50 ns unrestrained NPT following equilibration in order to determine if the ligand was stable. Any binding pose in which the ligand fully dissociated from the protein was not continued for the full 300 ns.

A similar procedure was used to generate starting binding configurations for the PTP1B-AB complex since there is no available crystal structure for AB in complex with PTP1B due to low solubility. For AB docking, the PTP1B structure used had a WPD loop in the open conformation and a disordered  $\alpha$ 7 helix. Both the originally generated structure and the centroid from clustering on backbone atoms of an apo trajectory were used to generate docking configurations. For each of the two structures, docking was performed in a 9 nm³ search space centered on the crystal binding site of AD to PTP1B since previous experimental results indicated a conserved binding location.  $^4$  These search space dimensions

adequately encompassed the allosteric site of PTP1B, as the maximum COM RMSD achieved by AD in complex with PTP1B was >1 nm and this volume encompassed the entirety of the surfaces presented by the  $\alpha 3$ ,  $\alpha 6$ , and  $\alpha 7$  helices. The 20 highest affinity binding modes were generated for each PTP1B configuration used, and as above, all of those determined to be distinct were chosen as initial configurations for MD simulations. This resulted in 9–11 binding locations depending on the PTP1B structure used for docking. As above, all binding poses in which the ligand fully dissociated from PTP1B during the initial 50 ns simulations were not continued for a full 300 ns trajectory.

Analysis of MD Trajectories. Before completing analysis on our MD trajectories in detail, we carried out two important processing steps: (i) removal of correlated trajectory frames and (ii) removal of unequilibrated trajectory frames and determination of convergence. Correlated trajectory frames were removed with ruptures 1.1.6,31 and unequilibrated trajectory frames were removed based on the root-meansquare deviation (RMSD) of backbone atoms, relative to the starting structure for the production simulation (further details in the previous work<sup>3</sup>). Following these processing steps, the number of uncorrelated frames per nanosecond ranges from 2 to 4 depending on the trajectory. This process could prevent the resolution of rare events; however, we verified that for all measurements (i.e., mean interaction frequency, h-bond occupancy, etc.), the mean value was not significantly different following the removal of uncorrelated frames. This process should thus increase only the accuracy of statistical uncertainty.

AD and AB exhibited several distinct bound conformations on PTP1B and TCPTP. In complex with PTP1B, both ligands bound to what we refer to as the  $\alpha$  site (Figure 3A). The  $\alpha$  site is defined as simultaneous contacts with helices  $\alpha 3$  and  $\alpha 7$ . The  $\alpha$  site encompasses both the loc1 and loc2 identified in our previous study; ligand oscillation frequency between the two sites was so high the two sites are unlikely to be kinetically distinct.<sup>3</sup> In contrast, in complex with TCPTP, both ligands bound to the  $\beta$  site, which is defined as simultaneous contacts with three structures: at least of the two  $\beta$  sheets in  $\beta 8-10$ , as well as the  $\alpha$ 3 helix (Figure 3B). The  $\beta$  site was identified from the trajectories of TCPTP in complex with both AD and AB. Of the 23 initial configurations simulated for the TCPTP-AD complex, only 6 remained in contact with the protein after the 50 ns evaluation simulation. Of these 6, two were bound in the region classified as the  $\beta$  site, and only one of the two was initiated near this site; one was bound to the  $\alpha$  site before becoming unstable after approximately 150 ns, and the remaining three sampled multiple binding locations but ended the trajectory dissociated from the protein. Of the 8 initial configurations simulated for the TCPTP-AB complex, 5 remained bound to the protein after the 50 ns evaluation simulation. Of these 5, three were bound in the region classified as the  $\beta$  site (only one was initiated there), and the other two sampled distinct alternate binding positions near the  $\alpha$ 4 helix. From the complex of TCPTP with AD and AB, the only conserved and repeatable binding location was the identified  $\beta$  site. This site is also identical to loc4 identified in our previous study from the binding of AD to PTP1B with a truncated  $\alpha$ 7 helix and it is overlapping with the 197-site identified by Keedy et al.<sup>32</sup> using a high-throughput fragment library search.

Both PTP1B and TCPTP have catalytically active and inactive states, in which the active conformation has a closed

WPD loop and an ordered  $\alpha$ 7 helix, while the inactive conformation has an open WPD loop and a disordered  $\alpha$ 7 helix. We classified the WPD loop conformation by the distance between the  $\alpha$  carbons of D181 and C215 for PTP1B and D182 and C216 for TCPTP (i.e., the catalytic acid and the nucleophile, respectively), 33-35 as measured using the compute distances function of MDTraj. A distance of >10 Å was defined as open, and otherwise the loop was defined as closed. This metric was explored and validated in our previous work.3 The width of the WPD loop was defined as the distance between  $C\alpha$  of residues 177–187 and 178–188 for TCPTP and PTP1B, respectively. The helicity of the  $\alpha$ 7 helix in our MD trajectories was quantified using the DSSP algorithm implemented in MDTraj 1.9.4.36 This algorithm characterizes the secondary structure of each residue based on the  $\phi$  and  $\psi$  torsional angles. This analysis allowed us to characterize the order or lack thereof of the  $\alpha$ 7 helix.

To further classify the structure of PTP1B throughout the simulations, we evaluated the RMSD of the backbone atoms and the root-mean-square-fluctuation (RMSF) of select protein regions relative to a centroid structure. We defined the centroid structure by clustering each trajectory on the backbone atoms of the equilibrated trajectory using gmx\_cluster and taking the centroid of the most populated cluster (consistently containing >90% of the trajectory). For ligand-bound trajectories, the center-of-mass (COM) RMSD for the ligand was also computed using bootstrapping on the uncorrelated configurations to determine the mean and standard error of the ligand COM RMSD value.

The catalytic domain of PTP1B has seven  $\alpha$  helices, several of which play important roles in allosteric communication. We quantified interhelical interactions and helix—ligand interactions between these influential helices as those with a residue—residue or residue-ligand distance of less than 4 Å. We defined interhelical interactions disrupted by ligand binding as those that occur significantly less (p < 0.05) in the ligand-bound vs corresponding apo conformation. We calculated the p-value using Welch's t test for the fraction of the simulation time that the interaction was present for the ligand-bound (AD or AB) compared to apo trajectories.

We isolated allosterically influential h-bonds with several steps. (i) We used the Baker-Hubbard model implemented within MDTraj to identify h-bonds. This model uses a proton donor-acceptor distance of 2.5 Å and a donor-acceptor angle of less than 120° to classify h-bonds. (ii) We removed h-bonds formed in a majority of all trajectories, regardless of the WPD loop conformation or the presence of an allosteric inhibitor, or formed between adjacent (within 3) residues and calculated the percent of the trajectory in which each of the remaining bonds appeared. (iii) For each h-bond, we determined the mean frequency formed for both apo WPD<sub>open</sub> and apo WPD<sub>closed</sub>. (iv) We identified bonds that showed a statistically significant (p < 0.01) difference between the groups. (v) Using our statistical threshold, we selected bonds that appeared more in either apo WPD<sub>open</sub> or apo WPD<sub>closed</sub> (with a minimum appearance of 70% in their primary state) to define h-bonding networks in each of these conformations. Notably, no h-bonds appeared significantly more or less frequently (given the above selection criteria) with ligands bound than in the apo WPD<sub>open</sub>

Computational Mutation Generation. A variety of mutations were made computationally for both PTP1B and TCPTP for validation of the simulation approaches by the

experiment. All mutant simulations involved the same protocol. Each mutation was created from the centroid of the most populated cluster obtained from the apo protein trajectory clustered on protein backbone atoms. The mutation itself was performed using Modeler 10.1, and then a 50 ns apo simulation was completed with each mutant in order to stabilize the structure. For TCPTP mutants, AD and AB were then placed in three different binding conformations all within the defined  $\beta$  site as described above. These three conformations were centroid structures from the trajectories with AD or AB bound to TCPTP. One trajectory was chosen at random, and the centroid of the trajectory was chosen as references. The other two centroids were from those trajectories that had the highest heavy-atom RMSD compared to the reference centroid to get a diversity of binding locations. For PTP1B mutants, AD and AB were placed using the same procedure but with binding sites within the previously defined  $\alpha$  site. 300 ns simulations were then performed of each mutant complex, and the time in nanoseconds for which the ligand remained bound to the defined site was evaluated and called the ligand retention time. The ligand COM RMSD was only calculated for the portion of the trajectory in which the ligand was bound to the  $\alpha$  site or  $\beta$  site for PTP1B and TCPTP, respectively.

**Experimental Methods.** *Materials.* We purchased yeast extract, sodium chloride, LB broth (Miller), potassium phosphate monobasic and dibasic, tris base, tetracycline hydrochloride, magnesium sulfate heptahydrate, imidazole, (4-(2-hydroxyethyl)-1-piperazineethanesulfonic acid) (HEPES), and premade 1 M HEPES buffer (pH 7.3) from Fisher; Triton X-100, tris(2-carboxyethyl)phosphine (TCEP), phenylmethylsulfonyl fluoride (PMSF), bovine serum albumin (BSA), p-nitrophenyl phosphate disodium salt hexahydrate (pNPP), and dimethyl sulfoxide (DMSO) from MilliporeSigma; Phusion and DNase I from New England Biolabs; agar and M9 salts from Becton Dickinson; glucose and Nalpha-4tosyl-L-arginine methyl ester hydrochloride (TAME) from Acros Organics; tryptone from Research Products International; isopropyl  $\beta$  D-1-thiogalactopyranoside (IPTG) from ChemCruz; kanamycin sulfate from IBI Scientific; carbenicillin from Gemini Bioproducts; lysozyme from Alfa Aesar; 10 kDa spin columns from Sartorius; 4-20% criterion TGX stain-free protein gels from Bio-Rad; and HisTrap and HiTrap columns from GE Healthcare.

Escherichia coli Strains. We used chemically competent NEB stable (no. C3040H) cells for cloning and NEB BL21(DE3) (no. C2527H) for protein overexpression.

Cloning and Molecular Biology. We constructed plasmids with Gibson assembly (50 °C for 1 h). Table S1 lists gene sources, and Table S2 lists primers used for site-directed mutagenesis.

Protein Expression and Purification. For this study, we used PTP1B<sub>1-321</sub> and TCPTP<sub>1-317</sub>, which are analogous truncations. These constructs are longer—and thus contain more of the full—length protein—than those used in other studies.<sup>37-39</sup> Each includes a catalytic domain (PTP1B<sub>1-298</sub> and TCPTP<sub>1-296</sub>), a disordered 20-residue stretch that extends beyond the  $\alpha$ 7 helix (PTP1B<sub>299-321</sub> and TCPTP<sub>297-317</sub>), and a C-terminal polyhistidine tag (LEHHHHHHH). We did not remove the His-tag during purification, but its appreciable distance from the binding sites and its identical position between the two PTPs make it an unlikely source of differences in potency between them. Prior work on both PTPs indicates

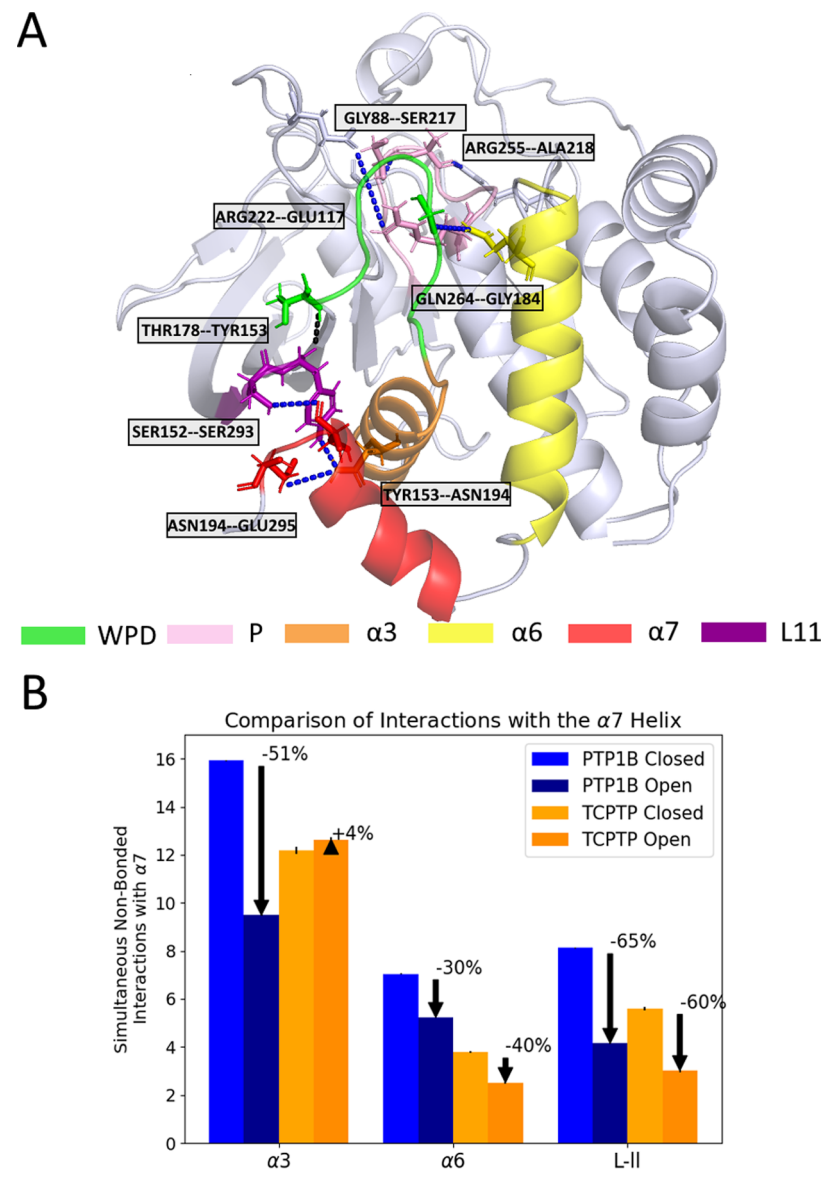


Figure 2. TCPTP possesses an allosteric network similar to that present in PTP1B (Figure S2). (A) In TCPTP, a h-bond network connects the WPD loop to the allosteric site. Each bond in this network involves residues homologous to those found in PTP1B.<sup>3</sup> (B) Disordering of the  $\alpha$ 7 helix in PTP1B and TCPTP disrupts several additional nonbonded interactions. This figure shows the number of nonbonded interactions present between the  $\alpha$ 7 helix and the  $\alpha$ 3,  $\alpha$ 6, and L-11 loop when the WPD loop is open and closed (when the  $\alpha$ 7 helix is disordered or ordered, respectively). The percentages reflect the percent difference in the number of interactions formed in the closed state over the open state. For PTP1B, the transition between these states disrupts the  $\alpha$ 3- $\alpha$ 7 interface, followed by the L-11- $\alpha$ 7 interface; for TCPTP, disruption is largely localized to nonbonded interactions at the L-11- $\alpha$ 7 interface. See Figure S6 for a diagram of disrupted interactions for TCPTP. Error bars represent standard error for n=3 MD trajectories.

that variants of different lengths prepared by different groups (e.g., PTP1B<sub>1-301</sub> with a cleaved His-tag and PTP1B<sub>1-321</sub> with a His-tag intact) have negligible differences in kinetic properties (i.e., a less than 2-fold change in  $k_{\text{cat}}$ ,  $K_{\text{M}}$ , or their ratio) so long as the  $\alpha$ 7 helix is included, as it is here. <sup>24,37</sup>

We overexpressed all proteins examined in this study in BL21(DE3) cells by carrying out steps described previously: (i) we used Gibson assembly to introduce mutations for PTP1B or TCPTP encoded by a pET16b vector and transformed sequence-confirmed plasmids into BL21(DE3) cells. (ii) We used an individual colony from each transformation to inoculate 20 mL of LB media, which we incubated at 37 °C in an incubator-shaker (225 rpm) for 6 h, prior to inoculating 1 L of rich induction media (20 g tryptone,

10 g yeast extract, 5 g sodium chloride, 50  $\mu$ g/mL carbenicillin, 72 mL 5X M9 salts solution, 20 mL of 20% glucose solution). (iii) We grew the resulting inoculum at 37 °C and 225 rpm. (iv) At an OD600 of 0.5–0.8, we added 500  $\mu$ M IPTG to induce protein expression and incubated the induced flasks at 22 °C and 225 rpm for 18–20 h. (v) We pelleted the final culture (5000 rpm for 10 min in a Beckman J2-HS floor centrifuge), disposed of the supernatants, and stored the cell pellets in a –80 °C freezer for future purification.

We purified PTP variants with fast protein liquid chromatography (FPLC) using previously described protocols. We lysed cells with chemical lysis buffer (for each gram of cell pellet, we used 4 mL of 20 mM tris base, 50 mM sodium chloride, 1% Triton X-100, and pH 7.5 supplemented with 2

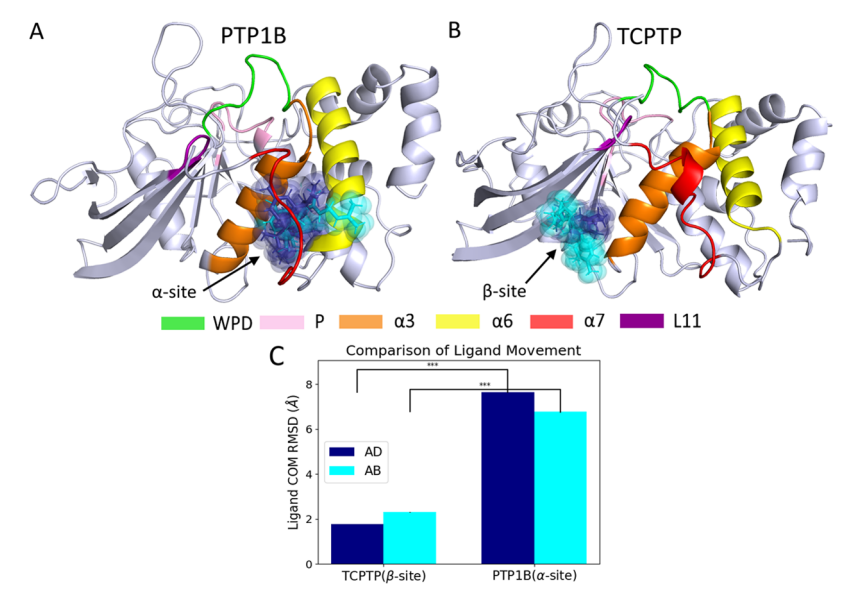


Figure 3. AD and AB bind to different sites on PTP1B and TCPTP. Spheres depict the centroid ligand conformation for each trajectory. (A) When AD (blue) and AB (cyan) bind to PTP1B with a disordered  $\alpha$ 7 helix, they primarily bind to the  $\alpha$  site, where they interact with the  $\alpha$ 3 and  $\alpha$ 7 helices. (B) When the same two ligands bind to TCPTP, they bind to the  $\beta$  site, where they interact with  $\beta$ 8–10 and the  $\alpha$ 3 helix. (C) Binding to the  $\alpha$ 3 site results in significantly higher COM RMSD than binding to the  $\beta$ 5 site because the ligands sample two regions of this site: one near the  $\alpha$ 6 helix and the other closer to the  $\alpha$ 3 helix. The  $\beta$ 5 site has a single dominant, though somewhat diffuse, binding mode. Error bars represent standard error for  $\alpha$ 5 and Trajectories.

mg of MgSO<sub>4</sub>–7H<sub>2</sub>O, 2 mg of TAME, 0.5 mL of TCEP (0.5 mM), 3.75  $\mu$ L PMSF solution, 1 mg of lysozyme, and 30 U of DNase), removed protein debris with saturated ammonium sulfate (20% for PTP1B variants and 10% TCPTP variants, respectively), and extracted the supernatant. We purified PTPs by using nickel affinity chromatography (HisTrap HP with 50 mM Tris–HCl, 300 mM sodium chloride, and 0.5 mM TCEP at pH 7.5 with and without 500 mM imidazole) followed by anion-exchange chromatography (HiTrap HP 5 mL with 50 mM HEPES, and 0.5 mM TCEP at pH 7.5 with and without 1 M NaCl). We concentrated final protein fractions into NaClfree anion-exchange buffer (10,000 kDa, Sartorius) and stored them in 20% glycerol at -80 °C.

Enzyme Kinetics. We characterized the activity of PTP variants on phosphate-p-nitrophenyl phosphate (pNPP). We used 96-well plates to prepare 200  $\mu$ L reactions with 50 nM of enzyme, 50  $\mu$ g/mL of BSA, and varying amorphadiene concentrations (0.5–500  $\mu$ M) in 50 mM HEPES buffer (pH = 7.3) with 10% DMSO. We incubated these plates for 1 h at room temperature (22 °C). We used 20 mM substrate (4nitrophenyl phosphate disodium salt hexahydrate) to initialize the reactions and monitored the formation of p-nitrophenol (pNP) by measuring absorbance at 405 nm at 30 s intervals over 8 min (SpectraMax iD3 plate reader). We used standard curves to convert absorbance measurements to product concentrations and used the slopes of the initial rate regime for Vo. We determined IC<sub>50</sub> estimates, in turn, via nonlinear regression (DataGraph) to the following equation:  $y = \min +$  $(\max - \min)/(1 + 10^{n \times (\log 10(x) - \log 10(ec_{50}))})$ , where min and max are the minimum and maximum percentages of activity remaining, n is the Hill coefficient, x is a substrate concentration associated with each percent activity y, and ec<sub>50</sub> is the half-maximal inhibitor concentration.

The  $IC_{50}$ s reported in this study differ from those reported in prior work; therefore, we will briefly comment: previously, we reported  $IC_{50}$ s for PTP1B and TCPTP of 53  $\pm$  8 and 349

 $\pm$  77  $\mu\rm M$ , respectively, with a ratio of 6.6  $\pm$  1.8. Here, we measured IC<sub>50</sub>s of 7.7  $\pm$  2.4 and 27  $\pm$  11.2  $\mu\rm M$ , respectively, with a ratio of 3.5  $\pm$  1.8. Study-to-study differences in the IC<sub>50</sub> ratio, our metric for selectivity, are not significant (p<0.01). Differences in the absolute IC<sub>50</sub>s, however, are significant (p<0.01) and probably reflect differences in the concentrations of amorphadiene in stock solutions, which were prepared fresh in each study. Critically, because we used the same stock solution for all measurements in this study, differences in our estimates of IC<sub>50</sub> reflect differences in the susceptibility of enzyme variants to inhibition.

# RESULTS

Allosteric Networks Are Similar betweeen PTP1B and **TCPTP.** Differences in the allosteric networks of PTP1B and TCPTP are a logical source of differences in the potency of AD and AB for these enzymes. 4 To map allosteric communication within PTP1B and TCPTP, we used MD simulations to identify networks of connected h-bonds whose presence was correlated to the WPD loop conformation. Indeed, PTP1B and TCPTP possess functionally similar allosteric systems (Figure 2A). Both proteins contain a conserved network of h-bonds that connect the active site (P-loop and WPD loop) to the allosteric site (L-11 loop,  $\alpha 3$ ,  $\alpha 6$ , and  $\alpha 7$  helices). These hbonds are present more frequently (p < 0.05) in the apo closed state than in the apo open state, an indication that they stabilize the closure of the WPD loop (Figure S2). In addition to their shared h-bonds, the PTP-specific sets of correlated hbonds include several distinct peripheral bonds. TCPTP has two additional h-bonds between the P-loop and adjacent residues, and PTP1B has one between the  $\alpha 6$  and  $\alpha 1$  helices (Figure S3). Though these bonds are present less often in the open conformation of both proteins (relative to the closed), their location and lack of connectivity to other bonds in the network suggest that they do not contribute to allosteric communication between the active and allosteric sites.

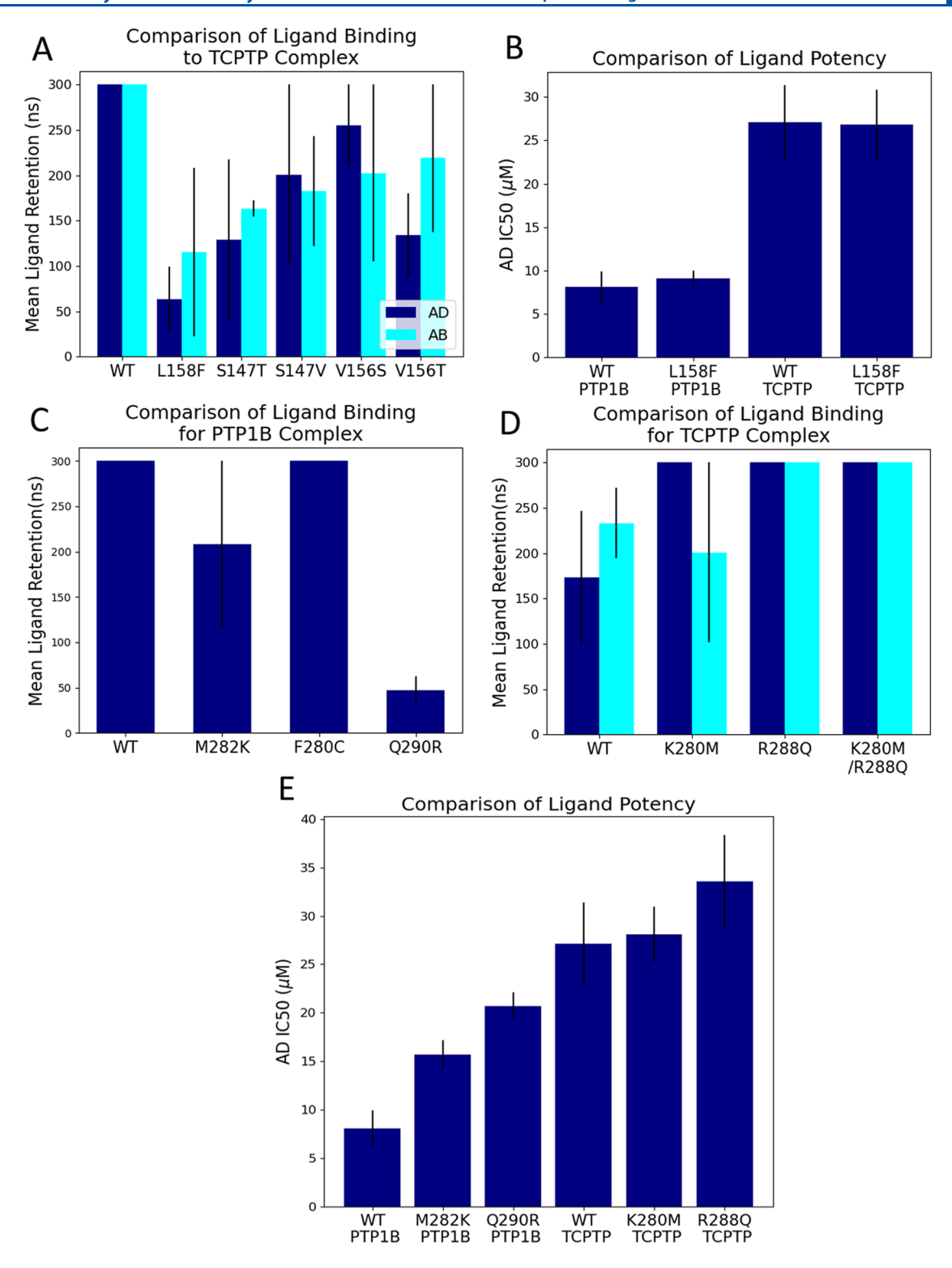


Figure 4. Mutations in the  $\alpha$  and  $\beta$  sites have different effects on terpenoid binding to PTP1B and TCPTP. (A) In MD simulations of TCPTP, mutations in the  $\beta$  site designed to disrupt binding reduced the mean ligand retention time for both AD and AB. Differences in retention time between mutants were not statistically significant (p < 0.05), a potential limitation of the 300 ns simulations. (B) Experimentally determined IC<sub>50</sub> values for AD-mediated inhibition were the same for both wild-type and L158F variants of PTP1B and TCPTP. The insensitivity for PTP1B, where AD binds to the  $\alpha$  site, is consistent with simulations, but the insensitivity for TCPTP, where simulations indicate that L158F reduces ligand retention time, is inconsistent with our hypothesis. (C, D) In simulations of AD binding, (C) mutations that made the  $\alpha$  site of PTP1B more like the  $\alpha$  site of TCPTP (M282 K, F280C, and Q290R) reduced ligand retention time. (D) Mutations that made the  $\alpha$  site of TCPTP more like the  $\alpha$  site of PTP1B (K280 M and R288Q), in turn, increased ligand retention time for both AD and AB. (E). Experimentally determined IC<sub>50</sub> values for AD-mediated inhibition of PTP1B suggest that M282 K and Q290R disrupt inhibition by this compound, a result consistent with simulations, but show that K280 M and R288Q in TCPTP have no perceptible effect, instead of increasing inhibition by stabilizing binding to the  $\alpha$  site. Error bars represent standard error for (A–D) n = 3 MD trajectories or (E) n = 3 technical replicates (dose–response curves appear in Figures S4 and S5).

In TCPTP, where allostery is less well studied, the h-bond network revealed by our MD simulations is consistent with published biochemical data, which shows reduced catalytic activity for the E295A variant of TCPTP. The individual network of the expression of TCPTP and in the h-bond connects the  $\alpha$ 7 helix to the remainder of the h-bond network, so its disruption should destabilize the closed conformation of PTP1B and decrease activity. The high similarity between the allosteric networks of PTP1B and TCPTP is also consistent with the decrease in activity observed when the  $\alpha$ 7 helix is removed from both enzymes (4-fold for TCPTP<sup>24</sup> and 3-fold for PTP1B<sup>37</sup>), in addition to prior work suggesting that allosteric communication is a conserved feature of PTPs. 10

The allosteric networks of PTP1B and TCPTP also contain nonbonded interactions that contribute to intramolecular communication, but the difference in the distribution of these interactions is unlikely to affect allosteric inhibition, as these interactions are not connected to the h-bond network. A cluster of van der Waals, h-bond, and salt bridge interactions near the C-terminus, for example, stabilizes the ordered  $\alpha$ 7 helix and allows the h-bond network to form (Figure S4). When we compare these interactions between the apo open and closed protein conformations, PTP1B shows an increase in disrupted interactions at the  $\alpha 3-\alpha 7$  interface, while TCPTP shows enhanced disruption at the L-11- $\alpha$ 7 interface (Figures 2B and S5). In both PTP1B and TCPTP, the  $\alpha$ 3 helix and L-11 loops help stabilize the  $\alpha$ 7 helix, with the most significant contribution from the  $\alpha$ 3 helix (Figure 2B). Given the difficulty of capturing the full ensemble for a disordered helix, it is possible that the  $\alpha 3-\alpha 7$  interface was not disrupted in our TCPTP simulations because the full ensemble was not sampled. Regardless, inhibitors bound to the allosteric site of PTP1B were previously shown to disrupt both the  $\alpha 3-\alpha 7$  and the L-11- $\alpha$ 7 interfaces, an indication that inhibition would still be effective on TCPTP from this site.3

Allosteric Ligands Bind to Different Sites on TCPTP and PTP1B. The similarity of the allosteric networks in PTP1B and TCPTP suggests that the previously reported differences in the potency of nonpolar terpenoid inhibitors result not from differences in allosteric communication with the active site but from differences in the binding process itself. MD simulations support this interpretation and suggest that AD and AB bind to alternate allosteric sites on the two PTPs. When bound to PTP1B, AD and AB bind to an  $\alpha$  site located between helices  $\alpha 3$  and  $\alpha 7$  (Figure 3A). By contrast, when bound to TCPTP, both ligands bind a separate, positionally distinct  $\beta$  site that sits at the interface of sheets  $\beta 8-\beta 10$  and helix  $\alpha 3$  (Figure 3B). Of the 14 initial binding poses determined for the TCPTP-AD complex, only two had AD in the  $\beta$  site. Over the course of 14 corresponding simulations, however, six resulted in stable AD binding to the  $\beta$ site (Figure S7A), seven caused AD to dissociate from TCPTP within 100 ns, and one resulted in stable binding to an alternative site. Of the seven initial poses for the TCPTP-AB complex, four simulations resulted in stable AB binding to the  $\beta$  site, and the remaining simulations caused AB to dissociate from the complex within 100 ns (Figure S7B). Intriguingly, the  $\alpha$  and  $\beta$  sites permit different amounts of ligand mobility: when bound to the  $\alpha$  site on PTP1B, AD and AB sample two neighboring sites and thus have a larger COM RMSD than when bound to the  $\beta$  site of TCPTP (Figure 3C). When bound to the  $\beta$  site of TCPTP, AB is more flexible than AD,

but both ligands occupy the same binding location and maintain conserved nonbonded interactions with TCPTP (Figure S8).

Binding to the  $\beta$  site on PTP1B is possible but with reduced binding affinity. In our previous analysis, we simulated the PTP1B-AD complex with a truncated  $\alpha$ 7 helix; for this truncation variant, AD occupied the  $\beta$  site (termed loc4 in this previous study) for 88% of observed trajectories compared to 0% occupancy in trajectories with a disordered  $\alpha$ 7 helix. This truncation-dependent binding is consistent with weaker binding to the  $\beta$  site, where residues are conserved between PTP1B and TCPTP. In kinetic assays, the potency of AD for the  $\alpha$ 7-less form of PTP1B was similar to its potency for TCPTP, a reduction in potency that further corroborates our interpretation that the  $\alpha$ 7 helix stabilizes binding to the  $\alpha$  site on PTP1B and that the secondary binding location is similar to that sampled in the TCPTP-AD complex.

Using molecular modeling, we identified several TCPTP mutations that disrupt binding to the  $\beta$  site while leaving the  $\alpha$  site unaffected. For this analysis, we selected mutations likely to disrupt binding to the  $\beta$  site but avoided charge-altering residues that might disrupt protein folding. In MD simulations of these mutations, the mutations L158F, S147T, S147V, V156S, and V156T reduced the ligand retention time at the  $\beta$  site of TCPTP, while analogous mutations in PTP1B had no effect on either ligand retention or COM RMSD at the  $\alpha$  site (Figures 4A and S9). The localized influence of these mutations suggests that their disruptive effect might serve as a diagnostic for detecting binding to the  $\beta$  site.

Our in vitro kinetic experiments indicate that mutations in the  $\beta$  site of TCPTP do not disrupt inhibition, which is a surprising result. In brief, for both PTP1B and TCPTP, we measured the IC $_{50}$  of AD, a readily synthesizable ligand with a crystallographically resolvable binding site. First, we examined wild-type and L158F mutants (Figures S10–S12). As this mutation reduced the ligand retention time for the  $\beta$  site of TCPTP, we expected that it would reduce binding and weaken inhibition for TCPTP but not PTP1B. In contrast to our hypotheses, the IC $_{50}$ s for AD were indistinguishable between wild-type and mutant enzymes (Figure 4B). Measurements of inhibition provide only an indirect—and substrate-sensitive—means of detecting changes in inhibitor binding, so there are a range of reasons why we might not see the expected effect, but additional alternative binding sites may be responsible.

Additional analyses suggest that the inhibition of TCPTP may be possible from an additional binding site, hereafter termed the  $\gamma$  site. We identified this peculiar site in our initial screens, where a single trajectory of the TCPTP-AD complex allowed AD to stably bind to this site (Figure S7). The  $\gamma$  site sits between the  $\alpha 3$  and  $\alpha 6$  helices and does not form nonbonded interactions with the  $\alpha$ 7 helix (Figure S13A). For AD complexes with both WT and L158F variants of TCPTP, AD remained bound to the  $\gamma$  site for the full 300 ns trajectory but exhibited a higher COM RMSD, relative to the  $\beta$  site (Figure S13B). As two out of the three initial binding configurations near the  $\gamma$  site reoriented to the  $\beta$  site, our simulations suggest that the  $\beta$  site might be more stable than the  $\gamma$  site. This finding, however, could reflect either (i) lower binding affinity for the  $\gamma$  site or (ii) the slow kinetics of exchange between sites, relative to the time scale of our simulations. In simulations of the PTP1B-AD complex with an ordered  $\alpha$ 7 helix, which disrupts the  $\alpha$  site, the  $\gamma$  site had a 24% occupancy, which is similar to that of the  $\beta$  site. This alternate

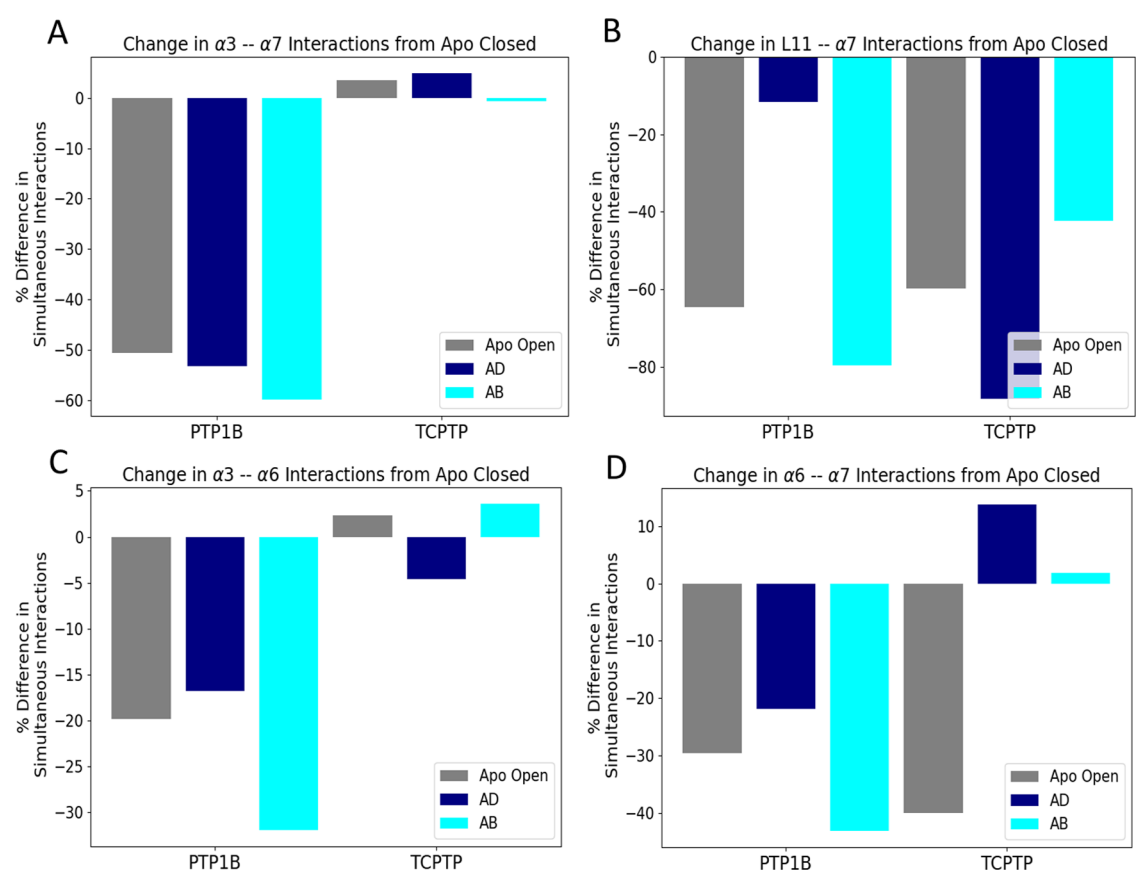


**Figure 5.** Binding to the  $\beta$  site of TCPTP has a distinct allosteric effect. (A) The binding of both AD and AB to the  $\alpha$  site of PTP1B disrupts the  $\alpha$ 3- $\alpha$ 7 interface relative to the interactions that form in the apo closed state. In TCPTP, neither the apo open nor ligand-bound states significantly change this interface, relative to apo closed. The  $\alpha$ 3 helix is responsible for over 50% of interactions that stabilize the ordered  $\alpha$ 7 helix in both PTP1B and TCPTP (Figure 2B). (B) In TCPTP, the apo open, AD-bound, and AB-bound states disrupt the L-11- $\alpha$ 7 interface; for PTP1B, only the apo open and AB-bound states are similarly disrupted. The L-11 loop is involved in ~25% of stabilizing interactions formed by the ordered  $\alpha$ 7 helix. (C,D) For PTP1B, the apo open, AD-bound, and AB-bound states disrupt (C) the  $\alpha$ 3- $\alpha$ 6 and (D) the  $\alpha$ 6- $\alpha$ 7 interfaces, where ligand binding to TCPTP has little effect. The  $\alpha$ 6 helix is involved in <20% of  $\alpha$ 7 helix stabilizing interactions. Notably, in this and previous studies, the  $\alpha$ 3- $\alpha$ 6 and  $\alpha$ 6- $\alpha$ 7 interfaces do not appear to contribute to the h-bond network, an indication that differences in these interfaces between PTP1B and TCPTP do not yield differences in allosteric communication in these two proteins.<sup>3,37</sup>

binding location, which is not affected by the presence of the L158F mutation, offers a potential rationale for the failure of this substitution to affect the  $IC_{50}$  of AD—though other stable sites could also contribute.

A comparison of residues that line the  $\alpha$  site of PTP1B and TCPTP indicates that minor sequence differences between PTP1B and TCPTP might destabilize the binding of AD and AB to TCPTP. Notably, prior biophysical analyses suggest that binding to the  $\alpha$  site of PTP1B can be stabilized by hydrophobic interactions with PHE280 and PHE196 and through additional nonbonded interactions with the  $\alpha$ 3 and  $\alpha$ 6 helices, primarily residues ALA189, ASN193, and SER295. 3,22 Of these residues, the  $\alpha$  site of TCPTP lacks only PHE280, but it includes several charged residues in place of less polar ones found in PTP1B (Figure S14A). These differences are likely to disrupt nonpolar interactions that allow AD and AB to bind to the  $\alpha$  site.

MD simulations support the theory that binding to the  $\alpha$  site of TCPTP is disrupted by charged residues that alter the hydrophobic pocket occupied by AD and AB in PTP1B. Starting with simulations of PTP1B, we introduced analogous residues from TCPTP in the  $\alpha$  binding pocket. Here, we sought to determine which nonconserved residues are responsible for destabilizing binding to the  $\alpha$  site in TCPTP.

As discussed above, we speculated that the F280C mutation might prevent hydrophobic interactions with AD and AB, while M282K and Q290R might disrupt nonbonded interactions within the hydrophobic pocket. Only the latter two mutations were sufficiently disruptive to cause ligand dissociation within 300 ns (Figure 4C). The reverse mutations in TCPTP (K280M and R288Q), in turn, increased the ligand retention time, an effect consistent with stronger binding at the  $\alpha$  site (Figure 4D). Although F280C was less impactful in PTP1B, it reduced stabilizing interactions and caused AD to move to the top of the pocket (Figure S15), potentially weakening binding and therefore allosteric inhibition. Overall, our simulations suggest that F280 helps anchor AD to the bottom of the  $\alpha$  site and indicate, more broadly, that disruption of the surrounding hydrophobic pocket in TCPTP destabilizes ligand binding to this site. Kinetic assaysof AD inhibition were largely consistent with the results of our MD simulations. As expected, the M282K and Q290R mutations in PTP1B reduced potency (i.e., increased IC<sub>50</sub>), an effect consistent with a reduction in binding stability (Figure 4E). The complementary mutations in TCPTP, however, had no effect on the IC<sub>50</sub> (Figure 4E); that is, they did not reduce the IC50, as we might expect from stronger binding to the  $\alpha$  site. The insensitivity of TCPTP to these

mutations suggests that the exchange of a single charged residue in TCPTP with its PTP1B equivalent is not sufficient to restore PTP1B-like binding affinity at the  $\alpha$  site. Differences in other residues or in the conformation of the  $\alpha$ 7 helix itself may also affect binding.

Inhibition at the  $\beta$  Site Has Different Effects than **Inhibition at the**  $\alpha$  **Site.** The binding of AD and AB to the  $\beta$ site of TCPTP produces distinct allosteric effects. When these terpenoids bind to the  $\alpha$  site of PTP1B, they disrupt interactions at the  $\alpha 3-\alpha 7$  and L-11- $\alpha 7$  interfaces; in doing so, they prevent ordering of the  $\alpha$ 7 helix and destabilize the hbond network required for the WPD loop closure (Figure 5A). Binding to the  $\beta$  site of TCPTP, by contrast, disrupts the L-11- $\alpha$ 7 interface, causes a slight increase (<5%) in the frequency of  $\alpha 3-\alpha 7$  interactions (Figure 5A,B), and induces a conformational change in the  $\alpha$ 3 helix that expands the WPD loop (i.e., the distance between the  $C\alpha$  carbons of residues 177-187 and 178-188 for TCPTP and PTP1B, respectively). The effect on the WPD loop is unusual. In the apo form of both PTPs, this loop expands by 2% when it opens (Figure S16). Binding to the  $\beta$  site broadens the open loop by an additional 7%, while binding to the  $\alpha$  site has a negligible effect on the loop width. The conformational change in the  $\alpha$ 3 helix is very slight (Figure S17A); ASN194 shifts by 1.5 Å and rotates by 40°, which elongates the donor-acceptor distance of TYR153-ASN194 and ASN194-GLU295 by 1.5 and 3.5 Å, respectively (Figure S17B,C). This elongation should increase the energetic cost of forming h-bonds between these residues, which participate in the h-bond network that forms when the WPD loop closes in the apo enzyme. This modest, yet disruptive effect may explain how AD and AB inhibit PTP1B when the  $\alpha$ 7 helix is removed, a truncation that directs them to the  $\beta$  site, and suggests, by extension, that binding to the  $\beta$  site may be less inhibitory than binding to the  $\alpha$  site, although this assessment requires a direct experimental comparison of inhibitors that bind to each of these sites with equal affinity.

#### DISCUSSION

Achieving selective inhibition within a highly conserved class of enzymes is difficult and requires extensive structural knowledge of both on- and off-targets and their known inhibitors. Previous studies have observed that both PTP1B and TCPTP exhibit correlated conformational changes in the WPD loop and  $\alpha$ 7 helix; when the WPD loop reorients from open to closed, the  $\alpha$ 7 helix folds to an ordered conformation from a disordered one. Our simulations build on this early work by comparing the h-bond networks of PTP1B and TCPTP; similar connectivity supports the theory that these two PTPs share a common allosteric system. <sup>10,22</sup> Our findings are important because they indicate that subtle differences in network residues or peripheral nonbonded interactions do not contribute to differences in the potency of allosteric inhibitors that bind to the same sites on these PTPs. For AD and AB, minor residue differences in the  $\alpha 6$  and  $\alpha 7$  helices direct inhibitor binding to different sites.

Previous studies of allosteric inhibitors of PTP1B have focused on the selectivity afforded by stable binding to the  $\alpha$  site. The potency and correspondingly slow off-rates of these compounds, however, have precluded the use of MD simulations to observe ligand movement to alternative sites. This study focuses on the selectivity afforded by low-affinity ligands that can sample multiple sites within the time scale of our simulations; it reveals a new mode of selective binding. On

PTP1B, the  $\alpha$  site allows for stable binding to a hydrophobic pocket, but on TCPTP, this site is disrupted by charged residues at position 290 and to a lesser extent, 282. Instead, they bind to the  $\beta$  site, which is conserved between the two PTPs; indeed, prior simulations of PTP1B suggest that binding is likely to occur at this site in the absence of the  $\alpha$ 7 helix, which enhances selectivity.<sup>3</sup> The results of a recent study indicate that more polar inhibitors can also bind to the  $\beta$  site of PTP1B, at least when its  $\alpha$ 7 helix is removed.<sup>41</sup> Our observations suggest that the  $\beta$  site of TCPTP contains a shared interaction that probably blunts the selectivity for one PTP over the other.

Our modeling results also provide direct evidence that inhibitors can modulate the allosteric networks of PTP1B and TCPTP through either (i) disruption of the  $\alpha 3-\alpha 7$  and L-11- $\alpha 7$  interfaces or (ii) rotation of the  $\alpha 3$  helix, which forces ASN194 of TCPTP into a position that strains the allosterically influential h-bond network. The first mechanism appears to be more disruptive than the second and may yield a more significant inhibitory effect; however, a rigorous exploration of this interpretation will require kinetic data on inhibitors with equal binding affinities but different disruptive mechanisms.

Broadly, our findings highlight the role of the  $\alpha$ 7 helix in enabling selective interactions and provide a framework for tuning the selectivity of inhibitors through focused interactions at the  $\alpha$  and  $\beta$  sites. Many promising allosteric inhibitors of PTP1B have large nonpolar surface areas and could exhibit similar binding behavior to TCPTP as the fully nonpolar fragments, AD and AB. The conserved allosteric network of PTP1B and TCPTP indicates that allosteric modulation of both proteins is possible; however, the results of the present study suggest that binding to the  $\alpha$  site is likely to be more selective for PTP1B. The design of selective inhibitors for TCPTP, in turn, may be more challenging, given the similarity of the  $\beta$  sites; however, compounds that exploit charged residues within the  $\alpha$  site or that interact with unique residues in the disordered region following the  $\alpha$ 7 helix, where sequence conservation is low, could offer a path forward.

# ASSOCIATED CONTENT

# Supporting Information

The Supporting Information is available free of charge at https://pubs.acs.org/doi/10.1021/acs.jpcb.3c03791.

Diagrams of helices; interhelical interactions; ligand binding locations; individual bond occupancies; RMSD and RMSF values;  $IC_{50}$  curves; and WPD loop width (PDF)

#### AUTHOR INFORMATION

## **Corresponding Authors**

Jerome M. Fox — Department of Chemical and Biological Engineering, University of Colorado Boulder, Boulder, Colorado 80309, United States; orcid.org/0000-0002-3739-1899; Email: jerome.fox@colorado.edu

Michael R. Shirts — Department of Chemical and Biological Engineering, University of Colorado Boulder, Boulder, Colorado 80309, United States; oorcid.org/0000-0003-3249-1097; Email: michael.shirts@colorado.edu

### **Authors**

Anika J. Friedman – Department of Chemical and Biological Engineering, University of Colorado Boulder, Boulder,

- Colorado 80309, United States; o orcid.org/0000-0002-5427-2779
- Hannah M. Padgette Department of Chemical and Biological Engineering, University of Colorado Boulder, Boulder, Colorado 80309, United States
- Levi Kramer Department of Chemical and Biological Engineering, University of Colorado Boulder, Boulder, Colorado 80309, United States
- Evan T. Liechty Department of Chemical and Biological Engineering, University of Colorado Boulder, Boulder, Colorado 80309, United States
- **Gregory W. Donovan** Department of Chemical and Biological Engineering, University of Colorado Boulder, Boulder, Colorado 80309, United States

Complete contact information is available at: https://pubs.acs.org/10.1021/acs.jpcb.3c03791

#### **Author Contributions**

A.J.F., J.M.F., and M.R.S. conceptualized the project. A.J.F. and M.R.S. designed the computational methodology, and E.T.L., L.K., G.W.D., and J.M.F. designed the experimental methodology. A.J.F. and H.M.P. performed and analyzed all molecular simulation experiments. A.J.F. wrote the original draft. H.M.P., J.M.F., and M.R.S. edited and reviewed the manuscript. L.K., G.W.D., and E.T.L. expressed and purified the proteins. L.K. performed molecular cloning and in vitro kinetic assays. J.M.F. and M.R.S. supervised the project and obtained the resources.

#### **Notes**

The authors declare the following competing financial interest(s): J.M.F. is a founder of Think Bioscience, Inc., which develops small-molecule therapeutics and employs J.M.F. and L.K., who are authors on this paper, and Matthew Traylor, immediately family of J.M.F. J.M.F. and L.K. also hold an equity interest in the company. Think Bioscience is exploring many possible drug targets, including protein tyrosine phosphatases. M.R.S. is an Open Science Fellow at and consultant for Psivant Sciences and consultant for Relay Therapeutics.

#### ACKNOWLEDGMENTS

This work was supported by funds provided by the University of Colorado Boulder (A.J.F, M.R.S., and H.M.P.), the National Institute of General Medical Sciences of the National Institutes of Health (E.T.L., R35GM143089), the National Science Foundation (J.M.F., CBET 1750244), and Think Bioscience (L.K.). This work utilized computational resources from the University of Colorado Boulder Research Computing Group, which is supported by the National Science Foundation (awards ACI-1532235 and ACI-1532236), the University of Colorado Boulder, and Colorado State University. This work also used the Advanced Cyberinfrastructure Coordination Ecosystem: Services and Support (ACCESS), which is supported by National Science Foundation grant number ACI-1548562. Specifically, it used the Bridges-2 system, which is supported by NSF ACI-1928147 at the Pittsburgh Supercomputing Center (PSC).

#### REFERENCES

(1) Houk, K. N.; Leach, A. G.; Kim, S. P.; Zhang, X. Binding Affinities of Host-Guest, Protein-Ligand, and Protein-Transition-State Complexes. *Angew. Chem., Int. Ed.* **2003**, *42*, 4872–4897.

- (2) Young, T.; Abel, R.; Kim, B.; Berne, B. J.; Friesner, R. A. Motifs for Molecular Recognition Exploiting Hydrophobic Enclosure in Protein— Ligand Binding. *Proc. Natl. Acad. Sci. U.S.A.* **2007**, *104*, 808–813.
- (3) Friedman, A. J.; Liechty, E. T.; Kramer, L.; Sarkar, A.; Fox, J. M.; Shirts, M. R. Allosteric Inhibition of PTP1B by a Nonpolar Terpenoid. *J. Phys. Chem. B* **2022**, *126*, 8427–8438.
- (4) Sarkar, A.; Kim, E. Y.; Jang, T.; Hongdusit, A.; Kim, H.; Choi, J.-M.; Fox, J. Microbially guided discovery and biosynthesis of biologically active natural products. *ACS Synth. Biol.* **2021**, *10*, 1505–1519.
- (5) Savjani, K. T.; Gajjar, A. K.; Savjani, J. K. Drug Solubility: Importance and Enhancement Techniques. *ISRN Pharm.* **2012**, 2012, No. 195727, DOI: 10.5402/2012/195727.
- (6) Hashemi, M.; Zandieh, M. A.; Talebi, Y.; et al. Paclitaxel and Docetaxel Resistance in Prostate Cancer: Molecular Mechanisms and Possible Therapeutic Strategies. *Biomed. Pharmacother.* **2023**, *160*, No. 114392, DOI: 10.1016/j.biopha.2023.114392.
- (7) Ma, N.; Zhang, Z.; Liao, F.; Jiang, T.; Tu, Y. The Birth of Artemisinin. *Pharmacol. Ther.* **2020**, 216, No. 107658, DOI: 10.1016/j.pharmthera.2020.107658.
- (8) Tautz, L.; Critton, D. A.; Grotegut, S. Protein Tyrosine Phosphatases: Structure, Function, and Implication in Human Disease. *Methods Mol. Biol.* **2013**, *1053*, 179–221, DOI: 10.1007/978-1-62703-562-0 13.
- (9) Cui, D. S.; Beaumont, V.; Ginther, P. S.; Lipchock, J. M.; Loria, J. P. Leveraging Reciprocity to Identify and Characterize Unknown Allosteric Sites in Protein Tyrosine Phosphatases. *J. Mol. Biol.* **2017**, 429, 2360–2372.
- (10) Hjortness, M. K.; Riccardi, L.; Hongdusit, A.; Zwart, P. H.; Sankaran, B.; De Vivo, M.; Fox, J. M. Evolutionarily Conserved Allosteric Communication in Protein Tyrosine Phosphatases. *Biochemistry* **2018**, *57*, 6443–6451.
- (11) Östman, A.; Hellberg, C.; Bohmer, F. D. Protein-tyrosine phosphatases and cancer. *Nat. Rev. Cancer* **2006**, *6*, 307–320.
- (12) Fuentes, F.; Zimmer, D.; Atienza, M.; Schottenfeld, J.; Penkala, I.; Bale, T.; Bence, K. K.; Arregui, C. O. Protein Tyrosine Phosphatase PTP1B Is Involved in Hippocampal Synapse Formation and Learning. *PLoS One* **2012**, *7*, No. e41536, DOI: 10.1371/journal.pone.0041536.
- (13) Zhu, Z.; Liu, Y.; Li, K.; Liu, J.; Wang, H.; Sun, B.; Xiong, Z.; Jiang, H.; Zheng, J.; Hu, Z. Protein Tyrosine Phosphatase Receptor U (PTPRU) Is Required for Glioma Growth and Motility. *Carcinogenesis* **2014**, 35, 1901–1910.
- (14) Mustelin, T.; Vang, T.; Bottini, N. Protein Tyrosine Phosphatases and the Immune Response. *Nat. Rev. Immunol.* **2005**, *5*, 43–57.
- (15) Zhang, C.; Wu, L.; Liu, X.; Gao, J.; Liu, S.; Wu, J.; Huang, D.; Wang, Z.; Su, X. Discovery of Novel PTP1B Inhibitors Derived from the BH3 Domain of Proapoptotic Bcl-2 Proteins with Antidiabetic Potency. ACS Med. Chem. Lett. 2021, 12, 1017–1023.
- (16) Ricke, K. M.; Cruz, S. A.; Qin, Z.; Farrokhi, K.; Sharmin, F.; Zhang, L.; Zasloff, M. A.; Stewart, A. F. R.; Chen, H.-H. Neuronal Protein Tyrosine Phosphatase 1B Hastens Amyloid  $\beta$ -Associated Alzheimer's Disease in Mice. *J. Neurosci.* **2020**, *40*, 1581–1593.
- (17) Begum, N.; Nasir, A.; Parveen, Z.; Muhammad, T.; Ahmed, A.; Farman, S.; Jamila, N.; Shah, M.; Bibi, N. S.; Khurshid, A.; Huma, Z.; Khalil, A. A. K.; Albrakati, A.; Batiha, G. E.-S. Evaluation of the Hypoglycemic Activity of Morchella Conica by Targeting Protein Tyrosine Phosphatase 1B. *Front. Pharmacol.* **2021**, *12*, No. 661803, DOI: 10.3389/fphar.2021.661803.
- (18) Figueiredo, A.; Leal, E. C.; Carvalho, E. Protein Tyrosine Phosphatase 1B Inhibition as a Potential Therapeutic Target for Chronic Wounds in Diabetes. *Pharmacol. Res.* **2020**, *159*, No. 104977, DOI: 10.1016/j.phrs.2020.104977.
- (19) Abdel-Magid, A. F. The Inhibitors of Protein Tyrosine Phosphatase Nonreceptor Type 2 (PTPN2) as Potential Enhancers of Cancer Immunotherapy and Type 1 (PTPN1) as Treatment of Metabolic Diseases. ACS Med. Chem. Lett. 2022, 13, 19–21.

- (20) Wiesmann, C.; Barr, K.; Kung, J.; Zhu, J.; Erlanson, D.; Shen, W.; Fahr, B.; Zhong, M.; Taylor, L.; Randal, M.; McDowell, R.; Hansen, S. Allosteric Inhibition of Protein Tyrosine Phosphatase 1B. *Nat. Struct. Mol. Biol.* **2004**, *11*, 730–737.
- (21) Zhang, Z.; Shang, Z.-P.; Jiang, Y.; Qu, Z.-X.; Yang, R.-Y.; Zhang, J.; Lin, Y.-X.; Zhao, F. Selective Inhibition of PTP1B by New Anthraquinone Glycosides from Knoxia Valerianoides. *J. Nat. Prod.* **2022**, *85*, 2836–2844, DOI: 10.1021/acs.jnatprod.2c00879.
- (22) Javier, G.-M. Computational Insight into the Selective Allosteric Inhibition for PTP1B versus TCPTP: A Molecular Modelling Study. *J. Biomol. Struct. Dyn.* **2020**, *39*, 5399–5410, DOI: 10.1080/07391102.2020.1790421.
- (23) Pedersen, A. K.; Peters, G. H.; Møller, K. B.; Iversen, L. F.; Kastrup, J. S. Water-molecule network and active-site flexibility of apo protein tyrosine phosphatase 1B. *Acta Crystallogr., Sect. D: Biol. Crystallogr.* **2004**, *60*, 1527–1534.
- (24) Singh, J. P.; Lin, M.-J.; Hsu, S.-F.; Peti, W.; Lee, C.-C.; Meng, T.-C. Crystal Structure of TCPTP Unravels an Allosteric Regulatory Role of Helix A7 in Phosphatase Activity. *Biochemistry* **2021**, *60*, 3856–3867.
- (25) Iversen, L. F.; Møller, K. B.; Pedersen, A. K.; Peters, G. H.; Petersen, A. S.; Andersen, H. S.; Branner, S.; Mortensen, S. B.; Møller, N. P. H. Structure Determination of T Cell Protein-tyrosine Phosphatase\*. *J. Biol. Chem.* **2002**, *277*, 19982–19990.
- (26) Abraham, M. J.; Murtola, T.; Schulz, R.; Páll, S.; Smith, J. C.; Hess, B.; Lindahl, E. GROMACS: High performance molecular simulations through multi-level parallelism from laptops to supercomputers. *SoftwareX* **2015**, *1*–2, 19–25.
- (27) Qiu, Y.; Smith, D. G. A.; Boothroyd, S.; et al. Development and Benchmarking of Open Force Field v1.0.0—the Parsley Small-Molecule Force Field. *J. Chem. Theory Comput.* **2021**, *17*, 6262—6280.
- (28) Bussi, G.; Donadio, D.; Parrinello, M. Canonical sampling through velocity rescaling. *J. Chem. Phys.* **2007**, *126*, No. 014101, DOI: 10.1063/1.2408420.
- (29) Schrödinger, LLC. The PyMOL Molecular Graphics System, Version 1.8, 2015.
- (30) Eberhardt, J.; Santos-Martins, D.; Tillack, A. F.; Forli, S. AutoDock Vina 1.2.0: New Docking Methods, Expanded Force Field, and Python Bindings. *J. Chem. Inf. Model.* **2021**, *61*, 3891–3898.
- (31) Truong, C.; Oudre, L.; Vayatis, N. Select review of offline change point detection methods. *Signal Process.* **2020**, *167*, No. 107299, DOI: 10.1016/j.sigpro.2019.107299.
- (32) Keedy, D. A.; Hill, Z.; Biel, J.; Kang, E.; Rettenmaier, J.; Brandao-Neto, J.; Pearce, N.; von Delft, F.; Wells, J.; Fraser, J.; Shan, Y. An expanded allosteric network in PTP1B by multitemperature crystallography, fragment screening, and covalent tethering. *eLife* **2018**, 7, No. e36307, DOI: 10.7554/eLife.36307.
- (33) Doncheva, N. T.; Klein, K.; Domingues, F. S.; Albrecht, M. Analyzing and Visualizing Residue Networks of Protein Structures. *Trends Biochem. Sci.* **2011**, *36*, 179–182.
- (34) Pettersen, E. F.; Goddard, T. D.; Huang, C. C.; Couch, G. S.; Greenblatt, D. M.; Meng, E. C.; Ferrin, T. E. UCSF Chimera-a Visualization System for Exploratory Research and Analysis. *J. Comput. Chem.* **2004**, *25*, 1605–1612.
- (35) Shinde, R. N.; Sobhia, M. E. Binding and discerning interactions of PTP1B allosteric inhibitors: Novel insights from molecular dynamics simulations. *J. Mol. Graphics Modell.* **2013**, 45, 98–110, DOI: 10.1016/j.jmgm.2013.08.001.
- (36) McGibbon, R. T.; Beauchamp, K. A.; Harrigan, M. P.; Klein, C.; Swails, J. M.; Hernández, C. X.; Schwantes, C. R.; Wang, L.-P.; Lane, T. J.; Pande, V. S. MDTraj: A Modern Open Library for the Analysis of Molecular Dynamics Trajectories. *Biophys. J.* **2015**, *109*, 1528–1532.
- (37) Choy, M. S.; Li, Y.; Machado, L.; Kunze, M.; Connors, C.; Wei, X.; Lindorff-Larsen, K.; Page, R.; Peti, W. Conformational Rigidity and Protein Dynamics at Distinct Timescales Regulate PTP1B Activity and Allostery. *Mol. Cell* **2017**, *65*, 644–658.

- (38) Torgeson, K. R.; Clarkson, M.; Kumar, G.; Page, R.; Peti, W. Cooperative dynamics across distinct structural elements regulate PTP1B activity. *J. Biol. Chem.* **2020**, 295, 13829–13837.
- (39) Krishnan, N.; Koveal, D.; Miller, D. H.; Xue, B.; Akshinthala, S. D.; Kragelj, J.; Jensen, M. R.; Gauss, C.-M.; Page, R.; Blackledge, M.; Muthuswamy, S. K.; Peti, W.; Tonks, N. K. Targeting the disordered C terminus of PTP1B with an allosteric inhibitor. *Nat. Chem. Biol.* **2014**, *10*, 558–566.
- (40) Li, X.; Wang, L.; Shi, D. The Design Strategy of Selective PTP1B Inhibitors over TCPTP. *Bioorg. Med. Chem.* **2016**, 24, 3343–3352.
- (41) Greisman, J. B.; Willmore, L.; Yeh, C. Y.; Giordanetto, F.; Shahamadtar, S.; Nisonoff, H.; Maragakis, P.; Shaw, D. E. Discovery and Validation of the Binding Poses of Allosteric Fragment Hits to PTP1b: From Molecular Dynamics Simulations to X-ray Crystallography. J. Chem. Inf. Model. 2023, 63 (9), 2644–2650.
- (42) Krishnan, N.; Konidaris, K. F.; Gasser, G.; Tonks, N. K. A Potent, Selective, and Orally Bioavailable Inhibitor of the Protein-Tyrosine Phosphatase PTP1B Improves Insulin and Leptin Signaling in Animal Models. *J. Biol. Chem.* **2018**, 293, 1517–1525.
- (43) Sharma, B.; Xie, L.; Yang, F.; Wang, W.; Zhou, Q.; Xiang, M.; Zhou, S.; Lv, W.; Jia, Y.; Pokhrel, L.; Shen, J.; Xiao, Q.; Gao, L.; Deng, W. Recent Advance on PTP1B Inhibitors and Their Biomedical Applications. *Eur. J. Med. Chem.* **2020**, *199*, No. 112376, DOI: 10.1016/j.ejmech.2020.112376.
- (44) Elhassan, R. M.; Hou, X.; Fang, H. Recent Advances in the Development of Allosteric Protein Tyrosine Phosphatase Inhibitors for Drug Discovery. *Med. Res. Rev.* **2022**, *42*, 1064–1110.